Journal of the Serbian Chemical Society
JSCS-info@shd.org.rs • www.shd.org.rs/JSCS
J. Serb. Chem. Soc. 84 (8) 819–836 (2019)
JSCS–5227
UDC 547.861+533.6.013.7:532.14+547.556.31
Original scientific paper

Vibronic and spin–orbit coupling effects in the absorption spectra of pyrazine: A quantum chemical approach

FABIAN DINKELBACH and CHRISTEL M. MARIAN*

Institute of Theoretical and Computational Chemistry, Heinrich-Heine-University Düsseldorf, Universitätsstraße 1, 40225 Düsseldorf, Germany

(Received 10 May, accepted 20 May 2019)

Abstract: Derivatives of dipole transition moments between spin–orbit coupled (SOC) multireference configuration interaction wave functions have been used in conjunction with vibrational frequencies from density functional theories to compute vibronic $S_1 \leftarrow S_0$ ($1^1B_{3u} \leftarrow 1^1A_g$) and $T_1 \leftarrow S_0$ ($1^3B_{3u} \leftarrow 1^1A_g$) absorption spectra in Herzberg–Teller approximation. The experimentally known spectra are well reproduced. The calculations reveal unexpectedly small spin–orbit couplings between the 1^3B_{3u} ($^3n\pi^*$) state and nearby optically bright $^1B_{2u}$ ($^1\pi\pi^*$) states, thus explaining the absence of the $1b_{1g}^1$ (ν_{10a}^1) fundamental in the vibrational fine-structure of the $T_1 \leftarrow S_0$ transition. Adiabatically, two triplet states are found below the S_1 state. The out-of-plane distorted T_2 minimum results from a pseudo Jahn–Teller interaction between two $^3\pi\pi^*$ states of B_{1u} and B_{2u} symmetry. At the D_{2h}-symmetric S_0 and S_1 minimum geometries, the latter states are located well above S_1. The S_1 and T_2 potentials intersect at geometries far away from the Franck–Condon region. This explains the apparently contradictory results that the linewidth in the higher energy regime above the $T_1 \leftarrow S_0$ origin suddenly broadens while no trace of a second triplet state, located energetically below the S_1 origin, could be identified in phosphorescence excitation spectra of the ultracold isolated pyrazine molecule.

Keywords: density functional theory; multireference configuration interaction; Herzberg–Teller coupling; singlet–triplet transitions; azabenzenes.

INTRODUCTION

Pyrazine (1,4-diazabenzene) is a prominent example where it has been proven necessary to go beyond the Franck–Condon approximation for understanding the intensity distribution in the $S_1 \leftarrow S_0$ absorption spectrum. Its first excited singlet state is of $n\pi^*$ type and known to borrow the intensity from higher-lying optic ally bright $\pi\pi^*$ states by vibronic coupling *via* the ν_{10a} (b_{1g}) and ν_5 (b_{2g}) vibrational modes. A comprehensive review of the experimental and theoretical knowledge on its vibronic spectra as of 1988 has been presented by Innes *et al.*[1]

* Corresponding author. E-mail: Christel.Marian@hhu.de
https://doi.org/10.2298/JSC190510048D

For the corresponding singlet–triplet absorption, similar vibronic activity might be expected as the vibrational frequencies in the first excited triplet state closely resemble those of S_1.[2] In contrast to the $S_1 \leftarrow S_0$ absorption, the $T_1 \leftarrow S_0$ phosphorescence excitation spectrum in a supersonic jet shows no evidence of strong vibronic coupling. Tomer *et al.*[3] report that the fundamental $\nu_{10a}^1 0^1$ and ν_{50}^1 transitions are absent in the $T_1 \leftarrow S_0$ spectrum. Instead, the overtones of ν_{10a} are seen in phosphorescence excitation spectra of neat crystals.[1] Another intriguing experimental result concerns the question whether one or two triplet states are located below S_1. Hochstrasser and Marzzacco[4] observed a sudden increase of bandwidth from 1 to 15 cm^{-1} in the singlet–triplet absorption spectrum of pyrazine crystals at 4.2 K, about 1600 cm^{-1} above the origin transition. Methylation of pyrazine in 2- and 6-positions lowers this threshold to about 50 cm^{-1} while tetramethylpyrazine shows only a diffuse spectrum. These results were interpreted as a manifestation of a perturbation on the $^3n\pi^*$ state by a $^3\pi\pi^*$ state that is located below the first excited singlet state and has some negligible electric dipole oscillator strength.[4] Resonance-enhanced multi-photon ionization experiments in supersonic jets point in the same direction. Villa *et al.*[5] were unable to induce one-colour photoionization of 2-methylpyrazine when the excitation energy was tuned to higher-lying vibronic levels of T_1. These authors consider displacements along a vibronically active out-of-plane coordinate, due to strong pseudo-Jahn–Teller distortion as a possible cause for the poor Franck–Condon factors aggravating the one-colour photoionization. However, no trace of a second triplet state, located energetically below the S_1 origin, could be found in phosphorescence excitation spectra of the ultracold isolated pyrazine molecule.[3] The signals appearing in the $T_1 \leftarrow S_0$ absorption spectra in this energy regime at higher temperatures were interpreted as hot bands of the $S_1 \leftarrow S_0$ absorption.[2,3,6]

So far, the quantum chemical simulations of the vibronic spectra of pyrazine focussed on the singlet absorption and fluorescence. Woywod *et al.*[7] employed a vibronic-coupling model Hamiltonian based on the Taylor expansion of diabatic potentials to model the absorption spectrum of the interacting S_1–S_2 manifold. Besides the S_1–S_2 coupling mode ν_{10a}, they took three totally symmetric tuning modes (ν_1, ν_{6a}, ν_{9a}) into consideration. Berger *et al.*[8] used a Herzberg–Teller expansion in all vibrational coordinates to model the S_0–S_1 absorption and fluorescence spectra at 0 and 300 K. Herein, the strongly anharmonic ν_{10a} coupling mode was expanded in terms of harmonic oscillators. Weber and Reimers[9] presented an extensive quantum chemical study on the vibrational frequencies in the T_1 state but did not address any spin-forbidden T_1–S_0 transitions. Siebrand and Zgierski[10] as well as Fischer[2] modelled the interaction between vibronic and spin–orbit coupling in pyrazine, but they had to estimate the magnitudes of the coupling matrix elements or treated them as fitting parameters.

The main focus of the present paper is on the apparent contradictions relating to the interpretation of the measured $T_1 \leftarrow S_0$ and $S_1 \leftarrow S_0$ spectra of pyrazine. In particular, we want to understand why the $T_1 \leftarrow S_0$ spectrum shows significantly less vibronic activity than the $S_1 \leftarrow S_0$ spectrum. Further, we will try to clarify the energetic position of the T_2 state and its possible role in the spectral broadening of the higher-lying $T_1 \leftarrow S_0$ bands. To this end, we will carry out the extensive quantum chemical calculations on the ground and electronically excited states of pyrazine including both vibronic and spin–orbit coupling effects.

THEORY AND COMPUTATIONAL METHODS

In the framework of the Franck–Condon (FC) approximation,[11,12] the transition moment, in an intensity calculation of molecular absorption or emission spectra, can be written as a simple product of an electronic term and FC factors depending solely on the vibrational degrees of freedom. For strong electronic transitions of polyatomic molecules, *e.g.*, spin-allowed ππ* transitions, this approximation is usually sufficient to describe the intensity distribution of the vibrational fine-structure of a band. The picture changes when it comes to the electronic transitions with small oscillator strengths, *e.g.*, nπ* excitations of heteroaromatic molecules, or if highly resolved spectra are to be interpreted. In this case, the transition moment cannot be considered independent of the nuclear motion and the coupling between the vibrational and electronic degrees of freedom, *i.e.*, vibronic coupling has to be taken into account in the modelling. For small triatomic and tetraatomic molecules, the sophisticated Hamiltonians have been worked out by Perić and co-workers[13-15] which include these couplings and are applicable to vibronic transitions involving even large-amplitude motions. In the more general case of polyatomic molecules, the formulation of such model Hamiltonians is too complicated and simpler strategies have to be pursued. One way to proceed is to follow the approach of Herzberg and Teller who formulated a coupling model in which the electric dipole transition moment is expanded about a reference point (typically the equilibrium geometry Q_0) as a function of the normal mode displacements, Q_k:[16]

$$\mu_{ij} = \mu_{ij}(Q_0) + \sum_k^N \left(\frac{\partial \mu_{ij}}{\partial Q_k} \right)_0 Q_k + \ldots \quad (1)$$

If the normal mode composition differs strongly between the initial and final states of the transition, it is wise to include Duschinsky effects[17] in the Herzberg–Teller (HT) treatment of the vibronic coupling.[18] A further complication arises if the initial and final states exhibit different spin multiplicities which is the case, *e.g.*, in singlet–triplet transitions. In these cases, an additional coupling term between the spin and spatial electronic angular momenta is required in the Hamiltonian to make the radiative transition allowed.[19] Perturbation theories addressing spin–forbidden radiative transitions by sum-over-states expressions are known to be slowly convergent with respect to the number of states included.[20] Here, we propose a conceptually simple, though resource-intensive way to include spin–orbit coupling and Herzberg–Teller coupling simultaneously. To this end, the spin–orbit-coupled correlated wave functions Ψ_i and Ψ_j and the corresponding electric dipole transition moments are generated by a variational multireference spin–orbit configuration interaction (MRSOCI)[21] procedure and the first derivative of the transition matrix element with respect to the dimensionless normal coordinate Q_k is calculated by finite differences:

$$\frac{\partial\left\langle\psi_i\left|\hat{\mu}\right|\psi_j\right\rangle|_{Q_0}}{\partial Q_k} \approx \frac{\left\langle\psi_i\left|\hat{\mu}\right|\psi_j\right\rangle|_{Q_0+\varepsilon\epsilon_k} - \left\langle\psi_i\left|\hat{\mu}\right|\psi_j\right\rangle|_{Q_0-\varepsilon\epsilon_k}}{2\varepsilon} \tag{2}$$

where ϵ_k denotes the unit vector in the direction of the normal mode Q_k and ε is the step length.

The electronic ground-state geometry of pyrazine was optimized at the level of density functional theory (DFT). For the optimization of the excited singlet states, the full linear response time-dependent density functional theory (TDDFT) was used, while the Tamm–Dancoff approximation (TDA) was employed for the triplet calculations.[22] Herein, the PBE0 density functional[23,24] in combination with a valence triple zeta basis set with polarization functions (TZVP)[25] was utilized. All structures were optimized starting with D_{2h}-symmetry constraints, while lowering the point-group symmetry if the stationary point turned out to be a saddle point. For an easier comparison with the experimental literature, the D_{2h}-symmetric molecule was chosen to lie in the *yz* plane, with the *z* axis running through the nitrogen centres. The geometry optimizations and the computation of two-electron integrals in a resolution-of-the-identity (RI) approximation were performed with the Turbomole 7.1 program package[26]. In the RI step, the auxiliary basis sets[27] optimized for Møller–Plesset calculations were engaged. The minima were verified by the numerical harmonic frequency analysis utilizing the SNF program.[28] The numerical frequencies were scaled by 0.9944 to account for systematic errors of the PBE0 functional.[29]

To calculate the vertical excitation energies, the dipole transition moments and the oscillator strengths at DFT or TDDFT optimized geometries, the DFT/MRCI method was used employing the original Hamiltonian developed by Grimme and Waletzke.[30,31] Herein, Kohn–Sham molecular orbitals (MOs) in conjunction with the BH-LYP density functional[32,33] serve as the one-particle basis. Secular equations for the electronic ground state and 40 excited singlet and triplet states, distributed equally over all irreducible representations, were solved. The DFT/MRCI wave functions were used to calculate spin–orbit coupling matrix elements (SOCMEs) utilizing the spin–orbit coupling kit (SPOCK)[34,35] developed in our laboratory. In SPOCK, an effective one-electron spin–orbit mean-field (SOMF) Hamiltonian[36] is used, which treats the two-electron interactions in a Hartree–Fock-like manner. Additionally, the one-centre atomic mean-field integral (AMFI)[37] approach is used to reduce the computational cost. The spin–orbit coupled wave functions for the lowest 20 states and their electric dipole transition moments, μ, in length form were determined using the DFT/MRSOCI method[21] implemented in SPOCK.

The first-order derivatives of the dipole transition moments, μ, at the ground state geometry were computed numerically. To this end, the minimum structure was distorted by ±0.1 units along the dimensionless normal modes. At each distorted geometry, DFT/MRCI and concomitant DFT/MRSOCI single-point calculations were carried out, followed by a computation of the dipole transition moment and its first derivative according to Eq. (2). A complication arises due to the fact that the phases of the matrix elements are arbitrary. They are determined by the phases of the wave functions Ψ_i and Ψ_j and of the MOs from which the determinants are constructed. These phases can change from point to point. Tatchen *et al.*[38] used the reference matrix elements involving a third, strongly coupling state to fix the phases of the matrix elements relative to the undistorted geometry. In the pyrazine case, the dipole transition matrix elements between the ground state (A_g) and the first excited singlet or triplet state (B_{3u}) are needed. For this combination of *gerade* and *ungerade* states, a reference state with two non-vanishing couplings could not be found. Therefore, we employed a more rigorous

approach to fix the phases. At each displaced geometry, the MO phases were set to match the ones of the equilibrium geometry. To accomplish this, we calculated the overlap matrix between both structures. The off-diagonal blocks of the overlap matrix easily show whether MOs changed their phases or switched their ordering. The phases of the DFT/MRCI wave functions were adjusted in such a way that the largest coefficient of each wave function is positive.

Franck–Condon and Herzberg–Teller absorption spectra were obtained by a Fourier transform approach implemented in the VIBES program.[39,40] In the calculation of the integrals over the vibrational wave functions of the initial and final states, a Duschinsky transformation[17] was applied. Temperature effects were included assuming a Boltzmann population of the vibrational levels in the initial state. Before the integration (time interval 5.5 ps, 2×10^5 grid points), the time correlation function was damped with a Gaussian of 5 cm^{-1} full width at half maximum.

RESULTS AND DISCUSSION

Electronic ground and excited states

Vertical and adiabatic DFT/MRCI excitation energies, computed at DFT/ /TDDFT converged geometries in D_{2h}-symmetry, are listed in Table I. The excited states of *gerade* symmetries have been omitted from this list because their electric dipole transitions from the ground state are forbidden in FC approximation and because they do not lie among the lowest singlet or triplet states. The T_1 (1^3B_{3u}) and S_1 (1^1B_{3u}) states correspond to nπ* excitations from the highest occupied molecular orbital (HOMO), an in-plane orbital of n/σ type, to the lowest unoccupied molecular orbital (LUMO) of π* type (Fig. 1). Their adiabatic energies are close to the experimental band origins.[1] This is also true for the optically bright ^{1}ππ* states, 1^1B_{2u} and 1^1B_{1u}, and the second *ungerade* ^{3}nπ* state, 1^3A_u. Note, however, that the D_{2h}-symmetric stationary points of the latter states

TABLE I. DFT/MRCI excitation energies compared with experimental results taken from Fischer[2]. Vertical excitation energies and oscillator strengths (in parentheses) are given at the ground state minimum

State	Character	$\Delta E_{DFT/MRCI}$ / eV			ΔE_{exp} / eV
		Vertical	Relaxed (D_{2h})	Adiabatic	
1^1A_g			0.00		0.00
1^3B_{3u}	n → π*	3.56	3.46	3.46	3.33
1^1B_{3u}	n → π*	4.03 (0.01102)	3.92	3.92	3.83
1^3B_{1u}	π → π*	4.39	3.93[a]	3.72 (C_1)	4.0
1^3B_{2u}	π → π*	4.34	4.17[a]		4.4
1^3A_u	n → π*	4.89	4.18[a]		4.2
1^1A_u	n → π*	4.97 (0.0)	4.29[a]	3.99 (C_{2h})	5.0
1^1B_{2u}	π→ π*	5.09 (0.10819)	4.82[a]		4.7
1^1B_{1u}	π→ π*	6.78 (0.09446)	6.46[a]	5.34 (C_1)	6.31
2^1B_{2u}	π→ π*	7.90 (0.57811)			
2^1B_{1u}	π→ π*	7.96 (0.62602)			
4^1B_{2u}	n→ σ*/Ry	8.62 (0.26377)			

[a]Saddle point

represent only the transition states. While the D_{2h}-constrained adiabatic excitation energies of all other states are within ≈ 0.2 eV of the experimental data, we notice an untypical deviation by ≈ 0.7 eV for the corresponding 1^1A_u (HOMO→ →LUMO+1) state. Because the $1^1A_u \leftarrow 1^1A_g$ transition is optically forbidden, the assignment of a broad band at approximately 5.0 eV in a near-threshold electron-energy loss spectrum was based on older MRCI calculations.[41]

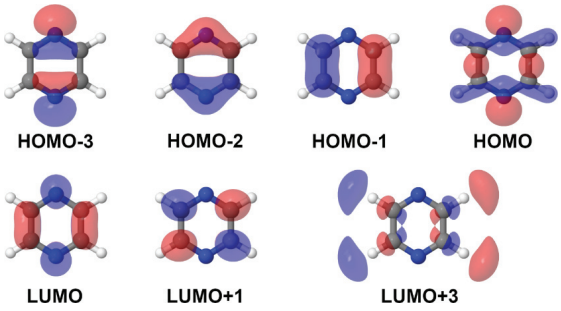

Fig. 1. Molecular orbitals at the ground state minimum relevant for spin–orbit coupling.

This energy regime corresponds roughly to the vertical excitation energy of this transition in our calculations. We also list vertical excitation energies of a few higher-lying bright singlet states which play a key role in the singlet-triplet absorption spectrum with regard to the intensity borrowing. The lowest $^1\pi\pi^*$ states have multiconfigurational character: 1^1B_{2u} and 2^1B_{2u} (HOMO-1→LUMO with admixtures of HOMO-2→LUMO+1 and *vice versa*), 1^1B_{1u} and 2^1B_{2u} (HOMO-1→LUMO+1 with admixtures of HOMO-2→LUMO and *vice versa*). 4^1B_{2u} represents a high-lying optically bright mixed $n\sigma^*$ and Rydberg state (HOMO→LUMO+3) which lends the intensity to the triplet absorption.

Using the D_{2h}-symmetry constraints, only the ^1A_g and $^3B_{3u}$ optimizations could be verified as minima. For the first excited singlet state, 1^1B_{3u}, one imaginary frequency was obtained for a b_{3g} mode. A scan of the energy profile along this mode revealed that the potential energy surface exhibits a shallow double well at the TDDFT level whereas a true minimum is found at the DFT/MRCI level. To obtain an estimate of the force constant of this mode, we used the curvature of the outer branches of the TDDFT scan to fit the harmonic frequency. Herein, the data with a distance of at least 3.5 units and at most 4.5 units away from the undistorted geometry were used. This fit yields a harmonic frequency of 1025 cm^{-1} for the $3b_{3g}$ mode which matches nicely the frequency of 1075 cm^{-1} in the related 1^3B_{3u} potential. The geometrical parameters of these minima may be found in Table II.

Further optimizations led to minimum structures for 1^3B_{1u}, 1^1A_u and 1^1B_{1u}. The molecule retains planarity in the 1^1A_u state, but in-plane movement of both nitrogen atoms in opposite directions lowers the symmetry towards C_{2h}. In the case of 1^3B_{1u} and 1^1B_{1u}, the symmetry is completely broken. In addition to an

asymmetric stretch of the C–N bonds, we observed a twist of the C–C bonds by about 30° on each side (Fig. 2, left). Its electronic structure points toward a pseudo Jahn–Teller rotation with the B_{2u} state (Fig. 2, right). Despite the out-of--plane distortion of the nuclear arrangement, the ππ* electronic character of the state is widely preserved.

TABLE II. Geometrical parameters of ground and first excited singlet and triplet state obtained with TDDFT (TZVP/PBE0)

State	CC / Å	CN / Å	CH / Å	∠ NCC / °	∠ CNC / °	∠ NCH / °
^1A_g	1.389	1.328	1.086	122.0	115.9	117.1
$^3B_{3u}$	1.389	1.335	1.084	120.0	115.9	117.1
$^1B_{3u}$	1.385	1.339	1.083	120.4	119.1	120.0
^1A_u (C_{2h})	1.413	1.289/1.362	1.089	122.0/116.2	121.8	120.2/122.0
$^3B_{1u}$ (C_1)	1.465	1.283/1.396	1.089/1.082	120.4/117.6	112.7	118.8/118.0
$^1B_{1u}$ (C_1)	1.452	1.301/1.372	1.089/1.085	117.4/116.2	112.8	119.3/117.9
Experiment[25]	1.403	1.339	1.115	122.2	115.6	113.9

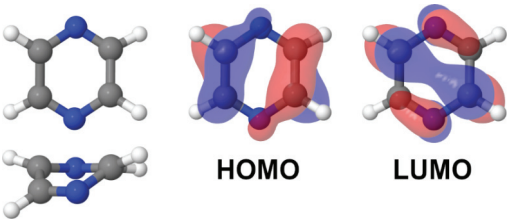

Fig. 2. Top and side view of the T_2 minimum structure (left) and molecular orbitals involved in the excitation at the T_2 minimum geometry (right).

The question, whether a second triplet state is located below or above the S_1 state, has been heavily debated in the literature.[2,3,4,5] Our DFT/MRCI calculations place the 1^3B_{1u} state ($^3\pi\pi^*$) state vertically ≈ 0.36 eV above the S_1 state in the FC region and ≈ 0.63 eV above the S_1 state at the S_1 minimum geometry. The geometry optimization in the T_2 potential leads to the highly distorted minimum (Fig. 2, left) with an adiabatic excitation energy ≈0.20 eV below the S_1 and ≈0.24 eV above the T_1 minimum. The latter value agrees well with the estimated T_2-T_1 splitting of 1600 cm^{-1} (≈0.20 eV), deduced by Hochstrasser and Marzzacco,[4] from the onset of the spectral broadening in their experiments. The presence of an intersection between the S_1 and T_2 potentials, far away from the FC region and the S_1 minimum geometry, provides a rationale for the conflicting experimental findings that (1) sharp absorption bands can be observed in a narrow energy regime above the origin of the $1^1B_{3u}\leftarrow1^1A_g$ transition and that (2) there is significant line broadening in the region between the S_1 and T_1 origins even at cryogenic temperatures[3,4] which precludes their assignment as hot bands of the $1^1B_{3u}\leftarrow1^1A_g$ absorption.

Vibrational frequencies

The calculated vibrational frequencies of the 1^1A_g ground state as well as the 1^3B_{3u} and 1^1B_{3u} excited states are generally in good agreement with the experi-

mentally obtained ones (Table III). An exception, relevant for the discussion of the vibronic spectra in the next section, is the $1b_{1g}$ (ν_{10a}) frequency in the 1^1B_{3u} state which is overestimated by 89 cm^{-1} relative to its experimentally deduced value of 383 cm^{-1}.

TABLE III. Vibrational frequencies of ground state and first excited singlet and triplet states compared to experimental values from Tomer *et al.*[4]; at the TDDFT level of theory, a saddle point and a shallow double minimum is obtained for this mode whereas DFT/MRCI shows a true minimum. Therefore, the frequency was fitted using the data from the outer branches of a TDDFT scan along the normal mode

Mode		^1A_g / cm^{-1}		$^1B_{3u}$ / cm^{-1}		$^3B_{3u}$ / cm^{-1}	
		Calc.	Exp.	Calc.	Exp.	Calc.	Exp.
$1a_u$	16a	340	342	419	400	440	400?
$1b_{3u}$	16b	430	416	228	237	261	237
$1a_g$	6a	607	597	618	585	619	620
$1b_{3g}$	6b	720	662	693	624	629	
$1b_{2g}$	4	773	705	502	552	405	557
$2b_{3u}$	11	801	791	726	577	729	563
$1b_{1g}$	10a	941	918	472	383	285	440
$2a_u$	17a	969	974	802	743	842	
$2b_{2g}$	5	974	757	805	518	823	522
$1b_{1u}$		1033		617		619	
$2a_g$	1	1052	1016	1040	970	1040	980
$1b_{2u}$		1096		1083		1087	
$2b_{1u}$		1173		1027		1026	
$2b_{2u}$		1246		1299		1318	
$3a_g$	9a	1257	1232	1197	1104	1201	1146
$2b_{3g}$		1371		1289		1304	
$3b_{2u}$		1446		1370		1364	
$3b_{1u}$		1520		1393		1399	
$3b_{3g}$		1605		1025*		1075	
$4a_g$	8a	1634	1579	1561	1377	1579	1230
$4b_{3g}$		3159		3164		3187	
$4b_{1u}$		3160		3174		3188	
$4b_{2u}$		3174		3196		3211	
$5a_g$		3180		3200		3214	

Berger *et al.*[8] have shown that it is necessary to go beyond the harmonic oscillator approximation to describe this vibration appropriately. Most frequencies vary only slightly among the three states. They can nevertheless appear prominently in the FC spectrum if their origins are markedly displaced. In a molecular transition in which the initial and final electronic states retain D_{2h} symmetry, this requirement can only be fulfilled by the totally symmetric (a_g) tuning modes. The modes $1b_{3u}$ (ν_{16b}), $1b_{2g}$ (ν_4), $1b_{1g}$ (ν_{10a}) and $3b_{3g}$ experience large frequency changes going from the ground state to the excited states. Their overtones are expected to be seen in the FC spectra, too. Moreover, the $1b_{1g}$ (ν_{10a})

and to a lesser extent also the $1b_{2g}$ (ν_4) and $2b_{2g}$ (ν_5) modes are made responsible for the strong vibronic coupling in the singlet moiety.[2,42] Since the frequency changes are similar in the 1^3B_{3u} potential, the question arises why their fundamentals are absent or at least very weak in the singlet-triplet absorption.[3,4]

$S_1 \leftarrow S_0$ absorption spectra

The FC and HT $S_1 \leftarrow S_0$ absorption spectra, calculated for 0 and 293 K, respectively, are shown in Fig. 3 and 4. The dipole transition moment of the $1^1B_{3u} \leftarrow 1^1A_g$ absorption has a value of $-0.33395ea_0$ in a FC approximation which is indicative of a moderately strong electronic transition. As expected for transitions between two D_{2h}-symmetric states, only totally symmetric modes, here $1a_g$ (ν_{6a}) and $3a_g$ (ν_9), generate high-intensity peaks in the FC spectrum. In addition, the overtones of $1b_{3u}$ (ν_{16b}), $1b_{1g}$ (ν_{10a}), and $1b_{2g}$ (ν_4) modes are visible. When HT coupling is switched on, additional transitions become symmetry-allowed. The derivatives of μ with respect to the vibronically most active modes are displayed in Table IV.

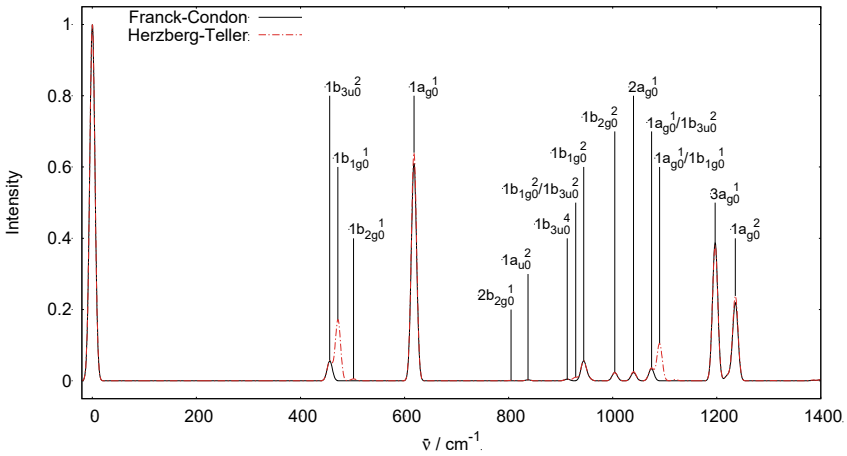

Fig. 3. Franck–Condon and Herzberg–Teller $S_1 \leftarrow S_0$ absorption spectra at 0 K.

The distortions along the $1b_{1g}$ (ν_{10a}) normal modes generate the by far largest gradients, explaining the intensity borrowing from the optically bright $1^1B_{2u} \leftarrow 1^1A_g$ and $2^1B_{2u} \leftarrow 1^1A_g$ excitations. The $1b_{1g0}^1$ (ν_{10a0}^1) fundamental and a $1a_{1g0}^1\ 1b_{1g0}^1$ ($\nu_{6a0}^1\ \nu_{10a0}^1$) combination transition are clearly visible in Fig. 3. Vibronic coupling to $^1B_{1u} \leftarrow 1^1A_g$ transitions via the $1b_{2g}$ (ν_4) and $2b_{2g}$ (ν_5) modes leads to the minor peaks in the HT spectrum. The a_g modes are HT active to a lesser extent. Their contributions cause small intensity changes of the FC allowed transitions only. Apart from the slight spectral shifts of the bands engaging the $1b_{1g}$ (ν_{10a}) mode, the agreement between the simulated 0 K spectrum (Fig. 3) and the supersonic jet spectrum of Tomer *et al.*[3] is very good, thus lending support to

our theoretical approach. When heating up to 293 K, hot bands appear near the 0-0 signal in the simulated spectrum (Fig. 4). These hot bands are also present in the vapour spectrum measured by Nakamura[6] at 300 K.

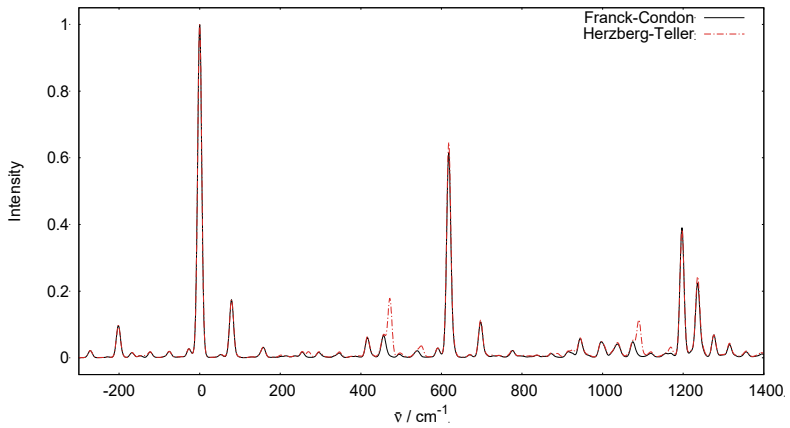

Figure 4. Franck-Condon and Herzberg-Teller $S_1 \leftarrow S_0$ absorption spectra at 293 K.

TABLE IV. Dipole transition moment derivatives (ea_0) for the $S_1 \leftarrow S_0$ transition at the ground state geometry

Mode k	Derivative		
	$\partial\langle {}^1B_{3u} \mid \mu_x \mid {}^1A_g\rangle/\partial Q_k$	$\partial\langle {}^1B_{3u} \mid \mu_y \mid {}^1A_g\rangle/\partial Q_k$	$\partial\langle {}^1B_{3u} \mid \mu_z \mid {}^1A_g\rangle/\partial Q_k$
$1a_g$	0.01009	0.0	0.0
$1b_{2g}$	0.0	0.0	0.04610
$1b_{1g}$	0.0	0.24924	0.0
$2b_{2g}$	0.0	0.0	0.01295
$2a_g$	0.00504	0.0	0.0
$3a_g$	0.00372	0.0	0.0
$4a_g$	0.02028	0.0	0.0
$5a_g$	0.00869	0.0	0.0

$T_1 \leftarrow S_0$ absorption spectra

When simulating the vibrational fine-structure of spin-forbidden radiative transitions, one must simultaneously account for spin–orbit, electric dipole and vibronic couplings.[10,19,43] To this end, we calculated the electric dipole transition moments of the multiplicity-mixed DFT/MRSOCI wave functions engaged in the $T_1 \leftarrow S_0$ absorption and their derivatives with respect to all normal modes. These data are sufficient for computing the vibronic singlet–triplet spectra, but they do not provide much qualitative insight. A detailed analysis of the direct and indirect contributions to the intensities will be presented after the discussion of the spectrum. The gradients of the dipole transition moments are all close to zero, indicating that vibronic coupling plays a minor role in the lower part of the

$T_1 \leftarrow S_0$ absorption spectrum. Accordingly, the FC and HT absorption spectra, displayed in Fig. 5, look basically the same. This finding is in agreement with the notion that all relatively intensive bands in the first 1250 cm^{-1} of the $T_1 \leftarrow S_0$ phosphorescence excitation spectrum, recorded by Tomer *et al.* in a supersonic jet, have been assigned to totally symmetric fundamentals, overtones and combinations.[3] We find only one noteworthy fundamental transition from a weakly active HT mode in the low energy regime of the spectrum around 400 cm^{-1} which we assign to $1b_{2g0}^{1}$ (ν_{40}^{1}). The overtone of that transition gives rise to a more intensive signal around 800 cm^{-1} for which the assignment by Tomer *et al.*[3] was uncertain. The peak at 880 cm^{-1} in the experimental spectrum is attributed to an overtone of the $1a_u$ (ν_{16a}) mode.

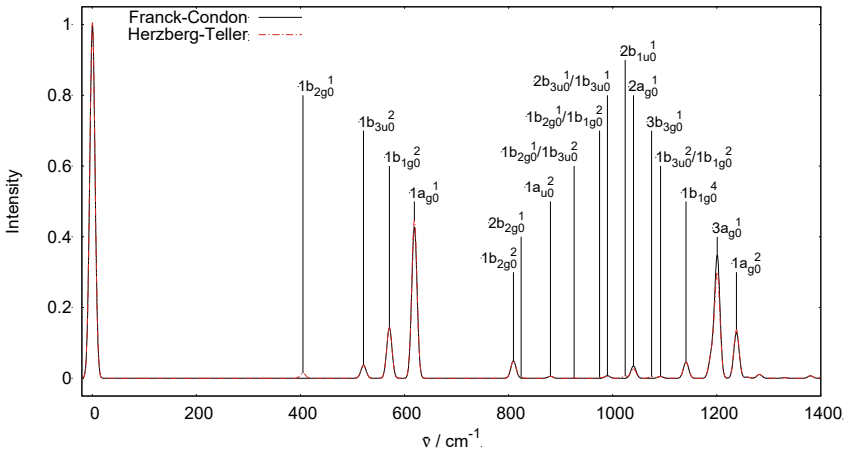

Fig. 5. Franck–Condon and Herzberg–Teller $T_1 \leftarrow S_0$ SOCI absorption spectrum at 0 K.

Consequently, the weak signal at 1114 cm^{-1} must have a different origin than the assignment (ν_{40}^{2}) proposed by Tomer *et al.* We found a combination band $1b_{3u0}^{2}\,1b_{1g0}^{2}$ ($\nu_{16b0}^{2}\,\nu_{10a0}^{2}$) in this energy regime. Most details of the measured phosphorescence excitation spectrum are well reproduced by our simulation, except for a signal at 570 cm^{-1} which arises from the $1b_{1g0}^{2}$ (ν_{10a0}^{2}) overtone and which is not observed in that experiment. At the same time, the intensity is missing in the $1a_{g0}^{1}$ (ν_{6a0}^{1}) signal at 620 cm^{-1}. While the frequency of the $1b_{1g}$ (ν_{10a}) mode was overestimated in the 1^1B_{3u} state, it appears to be underestimated in the 1^3B_{3u} potential by our calculations. If placed at slightly higher energy, its first overtone would overlay with the $1a_{g0}^{1}$ transition and recover the missing intensity of that signal. In addition, the second overtone $1b_{1g0}^{4}$ (ν_{10a0}^{4}) would be shifted to about 1200 cm^{-1} and add to the signal strength of the $3a_{g0}^{1}$ (ν_{9a0}^{1}) fundamental.

The leading terms of the DFT/MRSOCI wave functions and their projections onto the unperturbed DFT/MRCI states are shown in Table V. Under the influence of spin–orbit coupling, the 1^3B_{3u} state splits into three sublevels with an energy separation of less than 0.1 cm^{-1}. Their individual radiative singlet–triplet transitions are therefore spectrally not resolved.

TABLE V. Spin–orbit coupled states calculated by DFT/MRSOCI at the S_0 minimum geometry

State	Projection onto DFT/MRCI states	
	Largest triplet contributions	Largest singlet contributions
1	$1^3B_{1g}((m_s = 1) - (m_s = -1))$ $(8.0\times10^{-4}i)$	1^1A_g **0.99999**)
2	$1^3B_{3u}(m_s = 0)$ (**–0.99999*i***)	2^1A_u (-5.7×10^{-4})
3	$1^3B_{3u}((m_s = 1) + (m_s = -1))$ **(–0.69301 + 0.14049*i*)**	1^1B_{2u} $(1.3\times10^{-4} - 0.3\times10^{-4}i)$ 4^1B_{2u} $(-1.3\times10^{-4} + 0.3\times10^{-4}i)$
4	$1^3B_{3u}((m_s = 1) - (m_s = -1))$ **(0.00384 + 0.70710*i*)**	1^1B_{1u} (2.7×10^{-4}) 2^1B_{1u} (-4.0×10^{-4})
5	$1^3B_{1u}((m_s = 1) - (m_s = -1))$ $(2.9\times10^{-3}i)$ $2^3B_{1u}((m_s = 1) - (m_s = -1))$ $(1.4\times10^{-3}i)$ $1^3B_{2u}((m_s = 1) + (m_s = -1))$ (-7.8×10^{-4})	1^1B_{3u} **(-0.99999)**

Setting aside the triplet-triplet transitions, there are two symmetry-allowed pathways which do not involve vibronic activity. They are characterized by intensity borrowing from intermediate B_{1u} and B_{2u} singlet states. The third pathway *via* ^1A_u states is electric dipole forbidden in D_{2h} symmetry. We will therefore have a closer look at matrix elements of the type $\langle 1^3B_{3u}|H_{SO}|{}^1B_{1u}\rangle \langle {}^1B_{1u}|\mathrm{er}|1^1A_g\rangle$ and $\langle 1^3B_{3u}|H_{SO}|{}^1B_{2u}\rangle \langle {}^1B_{2u}|\mathrm{er}|1^1A_g\rangle$.

The lowest excited SOCI state consists mostly of the $m_s = 0$ component of the 1^3B_{3u} state. It exhibits A_u combined spatial and spin symmetry and is therefore not visible in the FC spectrum. The second excited SOCI state is dominated by the positive linear combination of the $m_s = 1$ and $m_s = -1$ spin components of the 1^3B_{3u} state. With the present choice of coordinate axes, this transition is *y*-polarized and borrows its intensity mainly from $^1B_{2u}$ states. Although the interacting states have different orbital characters and the coupling is allowed according to the El-Sayed rules,[44] the SOCMEs between the $^3n\pi$ state and the two lowest $^1\pi\pi^*$ states of B_{2u} symmetry are surprisingly small ($\langle 1^3B_{3u}|H_{SO}|1^1B_{2u}\rangle$ = = –1.63 cm^{-1}, $\langle 1^3B_{3u}|H_{SO}|2^1B_{2u}\rangle$ = 0.36 cm^{-1}). To rationalize this result, one must remember that the spin–orbit Hamiltonian is short-ranged and dominated by effective one-electron terms. The leading configurations of the 1^3B_{3u} and 1^1B_{2u} wave functions differ by a HOMO-1→HOMO single excitation and could hence be connected by a one-electron operator. Closer inspection of the involved orbitals (Fig. 1) reveals, however, that the HOMO-1 has a nodal plane running through the nitrogen atoms where the HOMO exhibits the largest amplitudes. The main configuration of the second singlet state in B_{2u} symmetry is doubly excited with respect to the dominant 1^3B_{3u} configuration. Their coupling would

require two-electron terms of the spin–orbit Hamiltonian which are much smaller than the effective one-electron terms. A medium-sized SOCME is found for the higher-lying 4^1B_{2u} state of $^1n\sigma^*$ type ($\langle 1^3B_{3u} | H_{SO} | 4^1B_{2u}\rangle$ = 5.28 cm^{-1}) which is connected to the 1^3B_{3u} state by a LUMO→LUMO+3 excitation in the orbital picture. The coupling is caused mostly by one-centre integrals between basis functions at carbon atoms, which are smaller than the corresponding integrals at nitrogen atoms, due to the reduced nuclear charge. The moderate spin–orbit interaction between the 1^3B_{3u} state and the $^1B_{2u}$ states is not the only reason why the transition to this triplet substate is very weak. The relative phases of the 1^1B_{2u} and 4^1B_{2u} coefficients in the second excited SOCI wave function are such that their dipole transition moments (Table VI) nearly cancel each other. The $T_1 \leftarrow S_0$ absorption and the corresponding phosphorescence derive their intensities nearly exclusively from *z*-polarized transitions to the third triplet sublevel. Its SOCI wave function is dominated by the negative linear combination of the $m_s = 1$ and $m_s = -1$ spin components of the $^3B_{3u}$ state. This substate mainly borrows intensity from the bright 1^1B_{1u} and 2^1B_{1u} states. Their spin–orbit interactions with the 1^3B_{3u} state are stronger than for the B_{2u}-symmetric $\pi\pi^*$ states ($\langle 1^3B_{3u} | H_{SO} | 1^1B_{1u}\rangle$ = = 6.89 cm^{-1}, $\langle 1^3B_{3u} | H_{SO} | 2^1B_{1u}\rangle$ = –13.97 cm^{-1}). The different magnitudes of the SOCMEs can be rationalized by investigating the MOs involved in the couplings. The two lowest $^1B_{1u}$ states are multiconfigurational states with major contributions from HOMO-1→LUMO+1 and HOMO-2→LUMO excitations. While the former represents a double excitation with respect to the leading HOMO→ →LUMO term of the 1^3B_{3u} state and does not couple *via* an effective one-electron operator, the latter is connected to 1^3B_{3u}, by a single excitation from HOMO-2 to HOMO. Their spin–orbit integral is quite large, as both MOs exhibit substantial amplitudes at the nitrogen atoms. The intensity contributions from the 1^1B_{1u} and 2^1B_{1u} states partially cancel each other as well, but the remainder is larger, owing to the larger weighting coefficient in the SOCI expansion and the substantial dipole transition moment of the $2^1B_{1u} \leftarrow 1^1A_g$ transition.

TABLE VI. DFT/MRCI dipole transition moments with respect to the electronic ground state

State	Dipole transition moment, ea_0
1^1B_{2u}	0.9316 (*y*)
4^1B_{2u}	1.1174 (*y*)
1^1B_{1u}	0.7543 (*z*)
2^1B_{1u}	1.7919 (*z*)

The intensity of the $1b_{1g}$ (ν_{10a}) fundamental in the $T_1 \leftarrow S_0$ spectrum is governed by matrix elements of the form[2,3,10] $\langle 1^3B_{3u} | H_{SO} | 1^1B_{2u}\rangle \langle 1^1B_{2u} | H_{vib} (b_{1g}) | 1^1B_{3u}\rangle \langle 1^1B_{3u} | er | 1^1A_g\rangle$ and $\langle 1^3B_{3u} | H_{vib} (b_{1g}) | 1^3B_{2u}\rangle \langle 1^3B_{2u} | H_{SO} | 1^1B_{3u}\rangle \langle 1^1B_{3u} | er | 1^1A_g\rangle$. The first spin–vibronic pathway via the $1b_{1g}$ (ν_{10a}) mode would engage the same small SOCME as the one involved in the direct SOC mech-

anism of the second triplet substate. The second spin–vibronic pathway involves the S_1 (1^1B_{3u}) state and the B_{2u} symmetric triplet state. The contributions of the 1^3B_{2u} substates to the SOCI wave function of the S_1 state are somewhat larger than those of the 1^1B_{2u} state in the T_1 wave function (Table V). Siebrand and Zgierski argued that the vibronic intensities induced via the two pathways might cancel out due to the interference.[10] We could not exclude this possibility, but we considered the electronic structures of the involved states and their weak SOC the main reason for the missing vibronic activity of the $1b_{1g}$ (ν_{10a}) mode in the $T_1 \leftarrow \leftarrow S_0$ spectrum. In accordance with that, we expected the much larger matrix elements of the form $\langle 1^3B_{3u} | H_{SO} | 1^1B_{1u} \rangle \langle 1^1B_{1u} | H_{vib}\ (b_{2g}) | 1^1B_{3u} \rangle \langle 1^1B_{3u} | \mathrm{er} | 1^1A_g \rangle$ and $\langle 1^3B_{3u} | H_{vib}\ (b_{2g}) | 1^3B_{1u} \rangle \langle 1^3B_{1u} | H_{SO} | 1^1B_{3u} \rangle \langle 1^1B_{3u} | \mathrm{er} | 1^1A_g \rangle$ to govern the intensity of the vibronic coupling *via* the $1b_{2g}$ (ν_4) and $2b_{2g}$ (ν_5) modes. We expected the vibronic coupling terms $\langle 1^1B_{1u} | H_{vib}\ (b_{2g}) | 1^1B_{3u} \rangle$ to be the limiting factors in these pathways because the frequency shifts of the b_{2g} modes were not very pronounced. Indeed, the traces of HT activity of the $1b_{2g}$ (ν_4) mode in the singlet-triplet absorption spectrum can be seen (Fig. 5) around 400 cm^{-1}.

We did not investigate the vibronic fine structure in the higher energy regime of the $T_1 \leftarrow S_0$ absorption. Our results suggest, however, that the nonadiabatic coupling between T_1 and the highly distorted T_2 (1^3B_{1u}) state, whose minima are located energetically below the S_1 minimum, will lead to the substantial broadening of the signals. Tomer *et al.*[3] did not find any evidence for a 1^3B_{1u} state in the phosphorescence excitation spectrum of the isolated pyrazine molecule. We explain this fact by the double-well shape of the T_2 potential with a saddle point at D_{2h}-symmetric structures and nearly vanishing 0-0 vibrational overlap between the 1^3B_{1u} and 1^1A_g states. This interpretation is also compatible with the lack of intensity in the one-colour photoionization spectrum of 2-methylpyrazine which was ascribed to be due to the poor Franck–Condon factors caused by pseudo-Jahn–Teller out-of-plane distortions.[5]

CONCLUSION

In the present work, we have studied the spectral properties of pyrazine by means of the high-level quantum chemical methods. In addition to the D_{2h}-symmetric T_1 and S_1 (B_{3u}, $n\pi^*$) minima, we find an out-of-plane distorted T_2 ($\pi\pi^*$) minimum with twisted C–C bonds and an unequal C–N bond lengths which is located adiabatically below the S_1 minimum. Its electronic structure is reminiscent of a mixture between two $^3\pi\pi^*$ wave functions of B_{1u} and B_{2u} symmetry. At the D_{2h}-symmetric S_0 and S_1 minimum geometries, the 1^3B_{1u} and 1^3B_{2u} states are located well above the S_1 state. The $^3\pi\pi^*$ states can interact vibronically with T_1 and *via* spin–orbit coupling with S_1. Among the spin–orbit interactions, the couplings between the B_{3u} and B_{1u} states prevail while the couplings between the B_{3u} and B_{2u} states are surprisingly small in comparison to their respective $n\pi^*$ and $\pi\pi^*$ orbital characters. The geometry relaxation in the T_2 potential leads to an

intersection with the S_1 potential energy surface at geometries far away from the Franck-Condon region. We have not quantitatively determined the energetic location of the conical intersection, but the presence of an energy barrier for the intersystem crossing from S_1 to T_2 qualitatively explains the following, apparently contradictory experimental observations that: a) sharp lines can be seen in the $S_1 \leftarrow S_0$ absorption spectrum close to the origin and no trace of a second triplet state could be identified in the phosphorescence excitation spectra of the ultracold isolated pyrazine molecule[3] whereas b) the linewidth of the $S_1 \leftarrow S_0$ absorption spectrum in the higher energy regime above the $T_1 \leftarrow S_0$ origin suddenly broadens.[4]

The dipole transition moments between the spin–orbit coupled multireference configuration interaction wave functions and their derivatives, with respect to all normal coordinates, have been used in conjunction with the vibrational frequencies from density functional theories to model the vibronic $S_1 \leftarrow S_0$ and $T_1 \leftarrow S_0$ absorption spectra in Franck–Condon and Herzberg–Teller approximation. The results of our study confirm that the vibronic coupling plays an important role in the $S_1 \leftarrow S_0$ absorption spectrum where the most prominent coupling modes are $1b_{1g}$ (ν_{10a}) and $1b_{2g}$ (ν_4). The low Herzberg–Teller activity of the $1b_{1g}$ (ν_{10a}) mode in the $T_1 \leftarrow S_0$ absorption and phosphorescence excitation spectra was traced back to the unexpectedly small $\langle 1^3B_{3u} \left| H_{SO} \right| 1^1B_{2u} \rangle$ and $\langle 1^3B_{3u} \left| H_{SO} \right| 1^1B_{2u} \rangle$ matrix elements. The $T_1 \leftarrow S_0$ absorption and the corresponding phosphorescence derive their intensities nearly exclusively from *z*-polarized transitions to the third triplet sublevel mainly represented by the negative linear combination of the $m_s = 1$ and $m_s = -1$ spin components of the $^3B_{3u}$ state. The intensity of the spin-forbidden transition is borrowed from the optically bright 1^1B_{1u} and 2^1B_{1u} states by a direct spin–orbit mechanism, without the necessity to invoke spin–vibronic coupling. The good agreement between our simulated spectra and the experimentally observed ones establishes confidence in the applied quantum methods and the procedures for computing vibronic spectra under the influence of spin–orbit coupling.

Acknowledgements. It is a pleasure to dedicate this article to Prof. em. Miljenko Perić (University of Belgrade) on the occasion of his 70th birthday. C.M.M. would like to thank him for his longstanding friendship and fruitful scientific collaborations.

ИЗВОД

ЕФЕКТИ ВИБРОНСКОГ И СПИН–ОРБИТНОГ СПРЕЗАЊА У АПСОРПЦИОНОМ СПЕКТРУ ПИРАЗИНА: КВАНТНО-ХЕМИЈСКИ ПРИСТУП

FABIAN DINKELBACH и CHRISTEL M. MARIAN

Institute of Theoretical and Computational Chemistry, Heinrich-Heine-University Düsseldorf, Universitätsstraße 1, 40225 Düsseldorf, Germany

Изводи диполних момената прелаза између таласних функција добијених помоћу спин–орбитно спрегнуте вишереферентне интеракције конфигурација коришћени су,

заједно са вибрационим фреквенцијама добијеним из теорије фунционала густине, да би се израчунао вибронски апсорпциони спектар $S_1 \leftarrow S_0$ ($1^1B_{3u} \leftarrow 1^1A_g$) и $T_1 \leftarrow S_0$ ($1^3B_{3u} \leftarrow 1^1A_g$) у Херцберг–Телер апроксимацији. Спектар добијен експерименталним путем је добро репродукован. Израчунавања откривају неочекивано мало спин-орбитно спрезање између 1^3B_{3u} ($^3n\pi^*$) стања и суседног оптички активног $^1B_{2u}$ ($^1\pi\pi^*$) стања, објашњавајући на тај начин одсуство $1b_{1g}^1 0$ (ν_{10a0}^1) фундаменталне вибрације у вибрационој финој структури $T_1 \leftarrow S_0$ прелаза. Адијабатски гледано, два триплетна стања се налазе испод S_1 стања. Налажење T_2 минимума ван равни је последица псеудо Јан–Телерове интеракције између два $^3\pi\pi^*$ стања B_{1u} и B_{2u} симетрије. При D_{2h}-симетричним S_0 и S_1 геометријама минимума, наведена стања се налазе знатно изнад S_1. S_1 и T_2 потенцијали се секу на геометријама које су знатно удаљене од Франк–Кондоновог региона. То објашњава наизглед контрадикторни резултат да се ширина линија у вишој енергетској области изнад $T_1 \leftarrow S_0$ почетка одједном увећава, док се друго триплетно стање, лоцирано енергетски испод S_1 почетка не може идентификовати у фосфоресцентном ексцитационом спектру ултрахладног изолованог молекула пиразина.

(Примљено 10. маја, прихваћено 20. маја 2019)

REFERENCES

1. K. K. Innes, I. G. Ross, W. R. Moomaw, *J. Mol. Spectrosc.* **132** (1988) 492 (https://dx.doi.org/10.1016/0022-2852(88)90343-8)
2. G. Fischer, *Can. J. Chem.* **71** (1993) 1537 (https://dx.doi.org/10.1139/v93-193)
3. J. L. Tomer, K. W. Holtzclaw, D. W. Pratt, L. H. Spangler, *J. Chem. Phys.* **88** (1988) 1528 (https://dx.doi.org/10.1063/1.454132)
4. R. M. Hochstrasser, C. Marzzacco, *J. Chem. Phys.* **49** (1968) 971 (https://dx.doi.org/10.1063/1.1670262)
5. E. Villa, M. Terazima, E. C. Lim, *Chem. Phys. Lett.* **129** (1986) 336 (https://dx.doi.org/10.1016/0009-2614(86)80354-2)
6. K. Nakamura, *J. Am. Chem. Soc.* **93** (1971) 3138. (https://dx.doi.org/10.1063/1.466618)
7. C. Woywod, W. Domcke, A. L. Sobolewski, H. J. Werner, *J. Chem. Phys.* **100** (1994) 1400 (https://dx.doi.org/10.1063/1.466618)
8. R. Berger, C. Fischer, M. Klessinger, *J. Phys. Chem., A* **102** (1998) 7157 (https://dx.doi.org/10.1021/JP981597W)
9. P. Weber, J. R. Reimers, *J. Phys. Chem., A* **103** (1999) 9830 (https://dx.doi.org/10.1021/JP991404K)
10. W. Siebrand, M. Z. Zgierski, *Chem. Phys. Lett.* **67** (1979) 13 (https://dx.doi.org/10.1016/0009-2614(79)87096-7)
11. J. Franck, *Trans. Faraday Soc.* **21** (1926) 536 (http://dx.doi.org/10.1039/tf9262100536)
12. E. U. Condon, *Phys. Rev.* **28** (1926) 1182 (https://dx.doi.org/10.1103/PhysRev.28.1182)
13. M. Perić, S. D. Peyerimhoff, R. J. Buenker, *Z. Phys., D* **24** (1992) 177 (https://dx.doi.org/10.1007/bf01426704)
14. M. Perić, F. Grein, M. R. J. Hachey, *J. Chem. Phys.* **113** (2000) 9011 (https://dx.doi.org/10.1063/1.1319645)
15. M. Perić, S. Jerosimić, M. Mitić, M. Milovanović, R. Ranković, *J. Chem. Phys.* **142** (2015) 174306 (https://dx.doi.org/10.1063/1.4919285)
16. G. Herzberg, E. Teller, *Z. Phys. Chem. Abt. B* **21** (1933) 410 (https://dx.doi.org/10.1515/zpch-1933-2136)
17. F. Duschinsky, *Acta Physicochim.* **7** (1937) 551
18. G. J. Small, *J. Chem. Phys.* **54** (1971) 3300 (https://dx.doi.org/10.1063/1.1675343)

19. C. M. Marian, in *Reviews in Computational Chemistry,* Vol. 17, K. B. Lipkowitz, D. B. Boyd, Eds., Wiley-VCH, New York, 1999, p. 99
20. S. R. Langhoff, E. R. Davidson, *J. Chem. Phys.* **64** (1976) 4699 (https://dx.doi.org/10.1063/1.432056)
21. M. Kleinschmidt, J. Tatchen, C. M. Marian, *J. Chem. Phys.* **124** (2006) 124101 (https://dx.doi.org/10.1063/1.2173246)
22. S. Hirata, M. Head-Gordon, *Chem. Phys. Lett.* **314** (1999) 291 (https://dx.doi.org/10.1016/S0009-2614(99)01149-5)
23. J. P. Perdew, K. Burke, M. Ernzerhof, *Phys. Rev. Lett.* **77** (1996) 3865 (https://dx.doi.org/10.1103/PhysRevLett.77.3865)
24. C. Adamo, V. Barone, *J. Chem. Phys*. **110** (1999) 6158 (https://dx.doi.org/10.1063/1.478522)
25. A. Schäfer, C. Huber, R. Ahlrichs, *J. Chem. Phys.* **100** (1994) 5829 (https://dx.doi.org/10.1063/1.467146)
26. *TURBOMOLE V7.1*, a development of University of Karlsruhe and Forschungszentrum Karlsruhe GmbH, 1989–2007, TURBOMOLE GmbH, since 2007; available from http://www.turbomole.com, 2017.
27. F. Weigend, M. Häser, H. Patzelt, R. Ahlrichs, *Chem. Phys. Lett.* **294** (1998) 143 (https://dx.doi.org/10.1016/S0009-2614(98)00862-8)
28. J. Neugebauer, M. Reiher, C. Kind, B. A. Hess, *J. Comput. Chem.* **23** (2002) 895 (https://dx.doi.org/10.1002/jcc.10089)
29. M. K. Kesharwani, B. Brauer, J. M. L. Martin, *J. Phys. Chem., A* **119** (2015) 1701 (https://dx.doi.org/10.1021/jp508422u)
30. S. Grimme, M. Waletzke, *J. Chem. Phys.* **111** (1999) 5645 (https://dx.doi.org/10.1063/1.479866)
31. C. M. Marian, A. Heil, M. Kleinschmidt, *WIREs Mol. Sci.* **9** (2019) e1394 (https://dx.doi.org/10.1002/wcms.1394)
32. A. D. Becke, *J. Chem. Phys.* **98** (1993) 1372 (https://dx.doi.org/10.1063/1.464304)
33. C. Lee, W. Yang, R. G. Parr, *Phys. Rev., B* **37** (1988) 785 (https://dx.doi.org/10.1103/PhysRevB.37.785)
34. M. Kleinschmidt, J. Tatchen, C. M. Marian, *J. Comput. Chem.* **23** (2002) 824 (https://dx.doi.org/10.1002/jcc.10064)
35. M. Kleinschmidt, C. M. Marian, *Chem. Phys.* **311** (2005) 71 (https://dx.doi.org/10.1016/J.CHEMPHYS.2004.10.025)
36. B. A. Heß, C. M. Marian, U. Wahlgren, O. Gropen, *Chem. Phys. Lett.* **251** (1996) 365 (https://dx.doi.org/10.1016/0009-2614(96)00119-4)
37. B. Schimmelpfennig, *AMFI is an atomic spin-orbit integral program,* University of Stockholm, 1996
38. J. Tatchen, N. Gilka, C. M. Marian, *Phys. Chem. Chem. Phys.* **9** (2007) 5209 (https://dx.doi.org/10.1039/b706410a)
39. M. Etinski, J. Tatchen, C. M. Marian, *J. Chem. Phys.* **134** (2011) 154105 (https://dx.doi.org/10.1063/1.3575582)
40. M. Etinski, V. Rai-Constapel, C. M. Marian, *J. Chem. Phys.* **140** (2014) 114104 (https://dx.doi.org/10.1063/1.4868484)
41. I. C. Walker, M. H. Palmer, *Chem. Phys.* **153** (1991) 169 (https://dx.doi.org/10.1016/0301-0104(91)90017-N)
42. M. de Groot, W. J. Buma, *J. Chem. Phys.* **127** (2007) 104301 (https://dx.doi.org/10.1063/1.2764075)

43. T. J. Penfold, E. Gindensperger, C. Daniel, C. M. Marian, *Chem. Rev.* **118** (2018) 6975 (https://dx.doi.org/10.1021/acs.chemrev.7b00617)
M. A. El-Sayed, *J. Chem. Phys.* **38** (1963) 2834 (https://dx.doi.org/10.1063/1.1733610).